CKT0353, a novel microtubule targeting agent, overcomes paclitaxel induced resistance in cancer cells

Jelena Dinić[1*], Carla Ríos-Luci[2], Ieva Karpaviciene[3], Inga Cikotiene[3], Miguel X. Fernandes[2], Milica Pešić[1], José M. Padrón[2*]

[1]Institute for Biological Research "Siniša Stanković", University of Belgrade, Bulevar despota Stefana 142, 11060 Belgrade, Serbia

[2]BioLab, Instituto Universitario de Bio-Organica "Antonio Gonzalez" (IUBO-AG), Centro de Investigaciones Biomédicas de Canarias (CIBICAN), Universidad de La Laguna, Avda. Astrofisico Francisco Sánchez 2, 38206 La Laguna, Tenerife, Spain

[3]Department of Organic Chemistry, Faculty of Chemistry, Vilnius University, Naugarduko 24, Vilnius LT 03225, Lithuania

***Corresponding authors**

Jelena Dinić, PhD

Institute for Biological Research "Siniša Stanković"

University of Belgrade

Bulevar despota Stefana 142, 11 060 Belgrade, Serbia

Tel.: +381 11 20 78 406

Email: jelena.dinic@ibiss.bg.ac.rs

ORCID ID: 0000-0003-3371-2381

José M. Padrón, PhD

BioLab

C/ Astrofísico Francisco Sánchez, 2

38206 La Laguna, Tenerife, Spain

Tel.: + 34 922 316 502 ext. 6126

Email: jmpadron@ull.es

Abstract

Microtubule targeting agents (MTAs) are extensively used in cancer treatment and many have achieved substantial clinical success. In recent years, targeting microtubules to inhibit cell division has become a widespread pharmaceutical approach for treatment of various cancer types. Nevertheless, the development of multidrug resistance (MDR) in cancer remains a major obstacle for successful application of these agents. Herein, we provided the evidence that CKT0353, α-branched α,β-unsaturated ketone, possesses the capacity to successfully evade the MDR phenotype as an MTA. CKT0353 induced G_2/M phase arrest, delayed cell division via spindle assembly checkpoint activation, disrupted the mitotic spindle formation and depolymerized microtubules in human breast, cervix, and colorectal carcinoma cells. Molecular docking analysis revealed that CKT0353 binds at the nocodazole binding domain of β-tubulin. Furthermore, CKT0353 triggered apoptosis via caspase-dependent mechanism. In addition, P-glycoprotein overexpressing colorectal carcinoma cells showed higher sensitivity to this agent when compared to their sensitive counterpart, demonstrating the ability of CKT0353 to overcome this classic MDR mechanism involved in resistance to various MTAs. Taken together, these findings suggest that CKT0353 is an excellent candidate for further optimization as a therapeutic agent against tumors with MDR phenotype.

Keywords: α-branched α,β-unsaturated ketones, anticancer activity, β-tubulin, microtubule targeting agents, multidrug resistance

Introduction

Microtubule targeting agents (MTAs) have been introduced as anticancer therapeutics several decades ago. These drugs exert inhibitory activity on cell proliferation mainly through blocking mitosis, which entails a precise control of microtubule dynamics and are commonly referred to as antimitotic drugs [1]. They bind to β-tubulin subunit on α/β-dimers which leads to disruption of microtubule dynamics, mitotic arrest and cell death [2]. MTAs with clinical importance are traditionally classified into two broad groups based on their mechanism of action: 1) microtubule stabilizing agents such as taxanes (paclitaxel – PTX, docetaxel) and epothilones; and 2) microtubule destabilizing agents such as colchicine, nocodazole (Noc), and vinca alkaloids (vinblastine, vincristine) [2]. Three well-established drug binding sites on β-tubulin include the vinca domain, the taxane site, and the colchicine site (also binding nocodazole) [3].

Drug resistance is one of the key factors obstructing the clinical applicability of microtubule targeting agents. One of the most comprehensively studied mechanisms of drug resistance is the overexpression of drug efflux pumps located in the plasma membrane, including P-glycoprotein (P-gp) and multidrug resistance-associated protein 1 (MRP1), members of a large ATP-Binding Cassette transporter family [4,5]. These membrane transporters represent a very efficient mechanism by which cancer cells attain resistance to various structurally and mechanistically unrelated drugs, a phenomenon known as multidrug resistance (MDR). MTAs are often substrates for P-gp which has been shown to actively extrude numerous hydrophobic drugs including vinca alkaloids, taxanes, and colchicine, changing their pharmacodynamics [6,7]. Moreover, MTAs are able to induce the expression of efflux pumps, particularly P-gp. Other key mechanisms behind the resistance of cancer cells to microtubule targeting agents include mutations at the drug binding sites that may have a negative impact on drug binding [8-12], altered microtubule dynamics [13], altered expression of different tubulin isotypes [14,15], and changes in microtubule-regulatory proteins [16,17].

Additionally, cancer cells may utilize defects in apoptosis pathways and cell cycle checkpoints as alternative mechanisms for evading the cytotoxicity of microtubule targeting chemotherapeutics. Discovering a new drug that modulates microtubule dynamics but has the ability to bypass the mechanisms of drug resistance is essential for successful anticancer therapy.

We previously reported the structure and synthesis of CKT0353 (Fig. 1a), an α-branched α,β-unsaturated ketone, prepared in a straightforward manner by the acid catalyzed coupling between arylalkynes and carbaldehydes [18]. This compound displayed significant antiproliferative activity against various human solid tumor cell lines including HBL-100 (breast), T-47D (breast), HeLa (cervix), SW1573 (lung), and WiDr (colon) [18].

In this study, we further investigated the mechanisms responsible for CKT0353 anticancer properties in HeLa and T-47D cells. In addition, to evaluate the ability of CKT0353 to evade the MDR phenotype, we employed an MDR and corresponding sensitive human cancer cell line, colorectal carcinoma DLD1-TxR and DLD1 [19]. Our findings suggest that CKT0353 acts as an MTA with striking effect on mitotic machinery whose pharmacokinetics is not affected by the MDR phenotype.

Materials and methods

Drugs

CKT0353, α-branched α,β-unsaturated ketone, was prepared and dissolved in dimethyl sulfoxide (DMSO) as previously described and stored at −20 °C [18]. Verapamil (VER), paclitaxel and nocodazole were purchased from Sigma (St Louis, MO).

Reagents

All starting materials were commercially available research-grade chemicals and used without further purification. RPMI 1640 medium was purchased from Flow

Laboratories (Irvine, UK), fetal calf serum (FCS) from Gibco (Grand Island, NY), while trichloroacetic acid (TCA) and glutamine were obtained from Merck (Darmstadt, Germany). Penicillin G, streptomycin, dimethyl sulfoxide (DMSO), 4',6-diamidino-2-phenylindole (DAPI), rhodamine 123 (Rho123), sulforhodamine B (SRB) and tetramethylrhodamine ethyl ester (TMRE) were purchased from Sigma (St Louis, MO).

Cell culture

Human solid tumor cell lines HeLa (cervix) and T-47D (breast) were a kind gift from Prof. G. J. Peters (VU Medical Center, Amsterdam, The Netherlands). Human colorectal carcinoma (DLD1) cell line was purchased from the American Type Culture Collection (Rockville, MD). P-glycoprotein (P-gp) overexpressing multidrug resistant DLD1-TxR cells were selected by continuous exposure to stepwise increasing concentrations of PTX from DLD1 cells [19]. All cell lines were maintained in 25 cm^2 culture flasks in RPMI 1640 supplemented with 5% heat inactivated FCS and 2 mM L-glutamine, 100 U/ml penicillin G, 0.1 mg/ml streptomycin at 37 °C in a 5% CO_2, 95% humidified air incubator. Exponentially growing cells were trypsinized and resuspended in antibiotic containing medium. Single cell suspensions displaying >97% viability by trypan blue dye exclusion were subsequently counted. After counting, dilutions were made to give the appropriate cell densities for inoculation onto 96-well and 6-well microtiter plates based on their doubling times.

Sulforhodamine B assay

The growth inhibition of DLD1 and DLD1-TxR cell lines was evaluated by sulforhodamine B assay. Cells were trypsinized, seeded into flat-bottomed 96-well microtiter plates at 4,000 cells/well and incubated overnight. Treatment with CKT0353 and nocodazole was performed in triplicate with six different concentrations (1 nM – 100 μM) and lasted 48 h. Following the treatment, cells were fixed in ice-cold 50% (w/v) trichloroacetic acid for 60 min at 4 °C, rinsed in tap water and stained with 0.4% (w/v) sulforhodamine B in 1% acetic acid for 15 min at room temperature. Cells were then

rinsed three times in 1% acetic acid to remove the unbound stain. The protein-bound stain was extracted with 150 µL 10mM Tris base (pH 10.5) per well. The optical density (OD) was read at 540 nm, with correction at 670 nm on a PowerWave XS Absorbance Microplate Reader (BioTek Instruments, VT, USA). Values were corrected for background OD from wells containing only medium.

Cell cycle analysis

HeLa, T-47D, DLD1 and DLD1-TxR cells were seeded in 6-well plates at a density of 0.5 × 10^6 cells/well. After 24 h, the approximate GI_{50} and $3xGI_{50}$ concentrations of CKT0353 (0.3 µM and 0.9 µM for HeLa and T-47D cells; 5 µM and 15 µM for DLD1-TxR cells; 10 µM and 30 µM for DLD1 cells) or nocodazole (0.1 µM and 0.3 µM for DLD1-TxR cells; 0.4 µM and 1.2 µM for DLD1 cells) were added to respective wells and incubated for an additional period of 24 h or 48 h. Cells were then trypsinized, harvested, transferred to test tubes (12 × 75 mm), and centrifuged at 1500 rpm for 10 min at 5 °C. The supernatant was discarded, and the cell pellets were resuspended in 200 µl of cold PBS and fixed by the addition of 1 ml ice-cold 70% EtOH. Fixed cells were incubated overnight at -20 °C followed by centrifugation at 1500 rpm for 10 min. The cell pellets were resuspended in 500 µl PBS. Then, 5 µl of DNAse-free RNAse (10 mg/ml) was added and the cell suspension was incubated in the dark at 37 °C for 30 min. After incubation, 10 µg/ml of propidium iodide (PI) was added. The mixture was incubated in the dark at room temperature for 15 min. Flow cytometric determination of DNA content (25,000 cells/sample) after CKT0353 treatment was analyzed on a BD Accuri™ C6 Flow Cytometer (BD Biosciences, New Jersey, USA). The fractions of the cells in G_0/G_1, S, and G_2/M phase were analyzed using BD Accuri™ C6 analysis software. Flow cytometric determination of DNA content after nocodazole treatment was performed on a FACSCalibur flow cytometer (Becton–Dickinson, Oxford, UK). Cell cycle distribution was determined in Summit v4.3 software (Dako, USA).

Cell death analysis

Cell death was analyzed using Annexin V-FITC apoptosis detection kit (BD Biosciences) according to manufacturer's instructions. HeLa and T-47D cells were seeded in 6-well plates at a density of 0.5×10^6 cells/well. After 24 h, 0.9 µM CKT0353 was added to respective wells and cells were incubated for an additional period of 6 h, 24 h, 36 h or 48 h. After treatment, cells were suspended in 100 µl of binding buffer containing 5 µl of Annexin V-FITC (AV) and 5 µl of propidium iodide (PI) and incubated for 15 min in the dark. Cells were then analyzed on a BD Accuri™ C6 Flow Cytometer (BD Biosciences, New Jersey, USA) using a FITC signal detector (FL1) and PI fluorochrome excited by 488 nm detectable by FL3. The experiments were repeated three times. A minimum of 100,000 events were assayed, and the percentages of viable (AV− PI−), early apoptotic (AV+ PI−), late apoptotic (AV+ PI+), and necrotic (AV− PI+) cells were analyzed by BD Accuri™ C6 analysis software.

Mitochondrial membrane potential analysis

To analyze the effect of CKT0353 on mitochondrial membrane potential, an early marker for apoptosis, the cell-permeant red-orange dye TMRE was used [20]. HeLa and T-47D cells were seeded in 6-well plates at a density of 0.5×10^6 cells/well. After 24 h, 0.9 µM CKT0353 was added to respective wells and cells were incubated for an additional period of 12 h, 24 h, 36 h or 48 h. Cells were stained with 0.5 µM TMRE (from 1 mM stock in DMSO) 30 min before the end of the experiment. After incubation, cells were trypsinized, harvested, transferred to test tubes (12 × 75 mm) and centrifuged at 200 × g for 5 min. Pellets were resuspended in 500 µL of PBS, vortexed and analyzed on a BD Accuri™ C6 Flow Cytometer. The loss of $\Delta\Psi_m$ was quantified by measuring TMRE fluorescence intensity in FL2 channel. A minimum of 100,000 events were assayed.

Rho123 accumulation assay

The ability of CKT0353 to inhibit the P-gp function was studied by Rho123 accumulation assay. Accumulation of Rho123, a P-gp substrate, was analyzed by flow cytometry utilizing the ability of Rho123 to emit fluorescence. The intensity of the

fluorescence is proportional to Rho123 accumulation in the cell. Verapamil, a well-known P-gp inhibitor, was used as a positive control. DLD1 and DLD1-TxR cells were grown to 80% confluence in 25 cm^2 flasks, trypsinized and resuspended in 10 ml centrifuge tubes in complete medium containing 5 µM Rho123. DLD1-TxR cells were then treated with 5 µM CKT0353 or 5 µM verapamil and both cell lines were incubated at 37 °C for 30 min. Cells were subsequently pelleted by centrifugation, washed with PBS and placed in cold PBS. The samples were kept on ice in the dark until the analysis on BD Accuri™ C6 Flow Cytometer (BD Biosciences, New Jersey, USA). The fluorescence of Rho123 was assessed at 530 nm. A minimum of 10,000 events were assayed for each sample.

Analysis of changes in cell morphology

HeLa and T-47D cells were suspended at 5×10^6 cells/flask and inoculated in 75 cm^2 flasks for 24 h. Cells were then exposed to 0.3 µM or 0.9 µM CKT0353 for 24 h or 48 h. At the end of treatment, the cells were examined and photographed under a phase-contrast microscope (Olympus CK-40 F-200).

Immunocytochemistry and confocal microscopy

For immunocytochemistry analysis, HeLa, T-47D, DLD1 and DLD1-TxR cells were seeded on glass coverslips (22 × 22 mm) placed at the bottom of 6-well plates and allowed to grow at 37 °C overnight before treatment. HeLa and T-47D cells were subsequently treated with 0.9 µM CKT0353 or 0.12 µM nocodazole. DLD1 and DLD1-TxR cells were treated with 5 µM and 15 µM CKT0353 (DLD1-TxR cells) or 10 µM and 30 µM (DLD1 cells) as well as 1 µM nocodazole. The treatments were carried out for 24 h and 48 h at 37 °C. All cell lines were then washed with PBS, fixed in 4% paraformaldehyde for 20 min at room temperature and blocked for 60 min with 0.5 % bovine serum albumin (BSA) in 0.3% Triton™ X-100 in PBS. To detect tubulin, mouse monoclonal anti-β-tubulin antibody (Sigma, St Louis, MO) was applied at 1:350 dilution in 0.5 % BSA/0.3% Triton X-100 and cells were incubated overnight at 4 °C. To detect Nup62, mouse anti-

nucleoporin 62 antibody (BD Biosciences, San Jose, CA) was applied at 1:400 dilution for at least 1 h at room temperature. After washing with PBS, secondary Alexa Fluor® 488 or Alexa Fluor® 568 goat anti-mouse IgG(H+L) antibodies (Thermo Scientific, USA) were applied at 1:1000 dilution in 0.5 % BSA/0.3% Triton X-100 for 120 min at room temperature protected from light. Nuclei were counterstained with DAPI or Hoechst 33342 (Sigma, St Louis, MO) for 15 min at room temperature and cells were mounted in Mowiol or Gelvatol (Sigma, St Louis, MO). Images were acquired on a Leica DMI4000 B confocal microscope (Leica Microsystems GmbH, Wetzlar, Germany) with a 40x objective using 405 nm and 488 nm lasers and analyzed with LAS-AF software.

Western Blot analysis

To prepare protein extracts for western blot analysis, HeLa and T-47D cells (2×10^6) were seeded in T 75 cm^2 flasks and grown until 60-70% confluence. Cells were then treated with CKT0353 for 6 h, 12 h, 24 h, 36 h or 48 h at 37 °C. After treatment, cells from each experimental group were harvested and centrifuged at 1200 rpm for 7 minutes. Cells were washed twice with cold PBS and lysed in ice-cold lysis buffer freshly supplemented with protease and phosphatase inhibitors (20 mM Tris pH 8.0, 140 mM NaCl, 1% NP- 40, 10% glycerol, 5 mM EDTA, 2 mM Na3VO4, 10 mM Na2P2O7, 10 mM NaF, 10 µg/mL aprotinin, 10 µg/mL leupeptin, 0.5 µg/mL pepstatin, and 1 mM PMSF). Lysates were incubated on ice for 10 min and then cell debris was spun down at 12,000 rpm for 10 min. After centrifugation, supernatants were transferred to new tubes and stored at -20 °C until used for SDS-PAGE gel. Protein concentration was determined by the Bradford method [21].

Equal amounts of protein were resolved by SDS/PAGE and electro-transferred onto PVDF membranes. Membranes were blocked in Tris-buffered saline with Tween (TBST; 100 mM Tris pH 7.5, 150 mM NaCl, 0.05% Tween 20) containing 1% of BSA for 1 h and then incubated 2-16 h with primary antibodies to PARP-1, Bcl-2, Mcl-1, Bcl-2, cyclin B1, Cdc2, pCdc2, CDK1, pCDK1, Wee1 (Santa Cruz Biotechnology, CA), caspase-3, active-

caspase-3, pRb (ser807/811), BubR1, pBuBR1, (BD Biosciences, San Jose, CA), caspase-7, caspase-9 (Cell Signaling, Danvers, MA), pH3 (ser 10) (Upstate, Cambridge, MA) as well as GAPDH and calnexin (Santa Cruz Biotechnology, CA) for loading controls for 2 h at room temperature. After washing three times with TBST, the membranes were then incubated for 30 min with the Horseradish peroxidase-conjugated secondary antibody (Goat Anti-rabbit IgG-HRP (Bio-Rad, Hercules, CA)), washed three times with TBST and bands were visualized by a luminol-based detection system with p-iodophenol enhancement. Western blots were repeated three times in each experimental condition.

Molecular modeling

The crystal structure of the colchicine pocket of α,β-tubulin (PDB ID: 3E22) was utilized as a template for docking studies using the program AutoDock Vina (The Scripps Research Institute, La Jolla, USA). Initial structures were drawn and minimized using AM1 semi-empirical method, with a gradient energy minimization method until the energy change between steps was lower than 0.01 kcal/mol (Hyperchem, Hypercube, USA). The algorithm used was the Polak-Ribiere (conjugate gradient). The best solution (based on docking score) was retained for further analysis. PyMol v1.5 (Schrödinger Inc, Portland, USA) was used for visualization and identification of residues in the binding pocket.

Results and discussion

CKT0353 causes morphological changes in cells

The biological effects of small molecules are generally reversible and rapid, and the degree of phenotypic effects in cells depends on the concentration of the small molecule. This can be used to generate dose-response data and offer greater confidence in the observed effect as it is more apparent. Thus, to better elucidate the mechanism

of action behind the cell growth inhibition induced by CKT0353, the approximate GI_{50} and $3xGI_{50}$ values were selected as low and high treatment concentrations, respectively.

Control HeLa and T-47D cells incubated in the presence of vehicle (0.5% (v/v) DMSO) grew as a monolayer with individual cells displaying typical shape. After 24 h of incubation with approximate GI_{50} or $3xGI_{50}$ concentrations (0.3 μM or 0.9 μM CKT0353)[18], both cell lines became less confluent, more rounded, and detached from the well suggesting an arrest in G_2/M phase of the cell cycle. These changes were also detected in both cell lines after 48 h exposure to CKT0353 (Online Resource 1 Fig. 1).

CKT0353 delays cell division via spindle assembly checkpoint activation

Detachment and round appearance of adherent tumor cells after CKT0353 treatment is commonly observed during mitosis. To analyze the effect of CKT0353 on cell cycle progression, HeLa and T-47D cells that are both hyperploid in nature were treated with 0.3 μM or 0.9 μM for 24 h and 48 h. Flow cytometric profiles (Fig. 1a) show that CKT0353 treatment induced a G_2/M arrest in both cell lines after 24 h. In HeLa cells, the G_2/M arrest continued throughout the experiment, but was accompanied by an increase in a sub-G_1 population at 48 h, indicating cell death (Online Resource 1 Fig. 2a). In T-47D cells, the G_2/M arrest continued throughout the experiment, with no evidence of significant cell death even after 48 h (Online Resource 1 Fig. 2a). As a notable number of live cells remained after the application of $3xGI_{50}$ concentration, it was used for treatment in subsequent experiments.

Furthermore, the observation of tetraploids in HeLa and T-47D cells after CKT0353 treatment indicated that cells managed to adapt and escape mitotic arrest by entering a tetraploid G_1 state without dividing, a phenomenon defined as mitotic slippage [22,23]. To confirm this, we examined the presence of nucleoporin 62 (Nup62) ring after 24 and 48 h of 0.9 μM treatment (Fig. 2a). Nup62 is a part of the nuclear pore complexes [24], responsible for the transportation between the nucleus and the cytoplasm. The nuclear pore complexes and the nuclear envelope dismantle in prophase

and subsequently reconstitute around the segregated chromosomes of daughter cells during telophase [25]. Compared to control, treated HeLa and T-47D cells exhibited chromosomal condensation and lacked Nup62 rings at 24 h, typically observed in cells blocked in prometaphase [26]. However, at 48 h a large number of cells entered a tetraploid G_1 state displaying a reconstituted Nup62 ring, uncondensed chromatin, and micronucleation. These findings demonstrated that treated cells overcame mitotic delay and arrested in a G_0–like state.

Cell cycle alterations upon CKT0353 treatment of HeLa and T-47D cells were additionally examined by western blot analysis (Fig. 2b). As CKT0353 induced an evident G_2/M arrest in both HeLa and T-47D cells, we assessed selected biochemical parameters involved in the G_2/M transition. To verify the entry of cells into mitosis, we examined the expression levels of mitotic markers pH3 and cyclin B1. Cyclin B1 is essential for mitotic initiation and its downregulation onsets the anaphase [27]. Mitosis entry was confirmed by the accumulation of both markers within 24 h. Treatment with CKT0353 increased the levels of pH3 at 12 h in both HeLa and T-47D cells, which subsequently decreased after 36 h and nearly disappeared at 48 h. Cyclin B1 levels gradually increased from 6 h to 12 h, followed by a decrease after 24 h of treatment (Fig. 2b).

BubR1 regulates the kinetochore-microtubule attachment [28]. Unattached kinetochores cause phosphorylated BubR1 to inhibit anaphase-promoting complex/cyclosome, activating the spindle assembly mitotic checkpoint and leading to a postponed progression into anaphase [29]. The presence of phosphorylated BubR1 strongly indicates that CKT0353-treated cells underwent a mitotic delay due to the spindle assembly checkpoint activation. Time-dependent phosphorylation of BubR1 indicated that CKT0353-treated cells entered mitosis and arrested the cell cycle in metaphase. Treatment of HeLa and T-47D cells with CKT0353 increased the levels of pBubR1 in a time-dependent manner within 24 h (Fig. 2b) indicating that the cells were unable to progress into anaphase. Phosphorylated BubR1 first appeared at 6 h, but later began to reduce at 36 h indicating an exit from mitosis.

After a mitotic delay the cells could complete cell division, but this is frequently accompanied by chromosome missegregation and aneuploidy [22]. Alternatively, cells can undergo mitotic slippage and return to interphase but with tetraploid nuclei [22,23]. Cells can then continue with the cell cycle, undergo cell death, or cell cycle arrest. Ultimately, a prolonged mitotic state can directly trigger cell death [30].

Reduced levels of pH3 and pBubR1 detected upon CKT0353 treatment accompanied by a prolonged mitotic arrest and polyploidy indicated that the cells possibly adapted. To confirm that HeLa and T-47D cells adapted and escaped mitotic arrest after CKT0353 treatment, we assessed the levels of hyperphosphorylated form of Rb (pRb), a G_0/G_1 cell cycle marker (Fig. 2b). This protein plays an essential role during G_1 phase progression [31]. Its hypophosphorylated form prevents the cell cycle progression, however during G_1 to S transition, pRb becomes hyperphosphorylated (Ser 807/811) and inactive. The inactive form is retained throughout the rest of the cycle and upon the completion of mitosis, pRb is dephosphorylated [31]. We observed increased levels hyperphosphorylated pRb after 12 h of CKT0353 treatment along with increased pH3 in both HeLa and T-47D cells. After 48 h, the hyperphosphorylated pRb levels were considerably decreased, indicating that cells exited mitosis without cytokinesis.

We further assessed the levels of Wee1 and cyclin-dependent kinase 1 (CDK1) (Fig. 2b). Wee1 kinase regulates the G_2/M cell cycle checkpoint by phosphorylating and inactivating CDK1, causing a delayed entry into mitosis [32]. In CKT0353-treated HeLa and T-47D cells, the levels of Wee1 and phosphorylated CDK1 (pCDK1) significantly reduced after 24 h, allowing the cells to overcome the mitotic delay.

CKT0353 triggers apoptosis via caspase-dependent mechanism

Cell cycle analysis revealed that HeLa cells showed a considerable sub-G_1 population after treatment with CKT0353. Accordingly, AV/PI apoptosis assay was used to further evaluate cell death in HeLa and T-47D cells after 24 h and 48 h of 0.9 µM treatment. CKT0353 application caused an increase of apoptotic and necrotic HeLa cells

in a time-dependent manner when compared to control cells. T-47D cells were less affected by the treatment (Fig. 3a). Time-dependent percentages of apoptotic and necrotic cells for both cell lines after treatment are given in Online Resource 1 Table 1. Considering that the permeability of the mitochondrial outer membrane changes during apoptosis, the ability of CKT0353 to modify the mitochondrial membrane potential ($\Delta\Psi_m$) through TMRE uptake was also examined (Fig. 3b). After 24 h of 0.9 µM treatment, TMRE fluorescence intensity began to decrease in a time-dependent manner, predominantly in HeLa cells.

Cells that die as a result of continued mitotic arrest most likely undergo apoptosis [33]. Analysis of biochemical parameters affected by this phenotype revealed that 0.9 µM CKT0353 treatment triggered the cleavage of PARP-1, caspase 3, caspase 7, and caspase 9 in HeLa cells after 24 h (Fig. 3c). Caspase 3 is the most active effector caspase, cleaved and activated by caspase 9 in the intrinsic pathway [34], and our findings indicate that CKT0353 application activates this apoptotic pathway.

The balance between pro-survival and pro-apoptotic Bcl-2 family members is known to modulate mitochondrial apoptosis [35]. Analysis by western blot showed that CKT0353 reduced the expression of anti-apoptotic Mcl-1 protein in both HeLa and T-47D cells at 24 h. In HeLa cells, the majority of Mcl-1 disappeared after 36 h, and was almost completely absent at 48 h. However, the expression levels of pro-survival protein Bcl-2 were increased in HeLa while a decrease was observed in T-47D cell line after 24 h (Fig. 3c). These data suggest that sensitivity of different cells to apoptotic stimuli is partly regulated by the interaction between the pro-apoptotic and anti-apoptotic Bcl-2 family members and this may contribute to the observed effect on $\Delta\Psi_m$-induced cell death.

CKT0353 disrupts the mitotic spindle formation

During cell division, a dynamic reorganization of the microtubules enables the mitotic spindle formation as a key step during chromosome segregation into daughter cells [36]. To better understand the effect of CKT0353 on the mitotic machinery, we

examined perturbations of mitotic spindles in HeLa and T-47D cells. Both cell lines were treated with 0.9 μM CKT0353 for 24 h or 48 h and stained with anti β-tubulin antibody. Untreated cells in interphase displayed typical microtubules while mitotic cells had well-organized bipolar spindles with condensed chromosomes in the metaphase plates (Fig. 4). CKT0353 treatment caused tubulin depolymerization in both cell lines after 24 h, as well as abnormal appearance and position of mitotic spindles, suggesting the cells were arrested in prometaphase. At 48 h, multinucleated interphase cells were observed. Hyperploid formation in HeLa and T-47D cells treated with CKT0353 implies that the cells exited mitosis via mitotic slippage. The observed effects were compared to a well-known tubulin depolymerization agent nocodazole. Cells treated with nocodazole enter mitosis but do not form metaphase spindles as microtubules cannot polymerize [37]. As a result, the cells arrest in prometaphase upon spindle assembly checkpoint activation. HeLa and T-47D cells were treated with 0.12 μM Noc for 24 h which resulted in complete dissolution of the mitotic spindle, in a similar manner to CKT0353 treatment (Fig. 4).

CKT0353 affects tubulin dynamics via binding to nocodazole site

Both CKT0353 and nocodazole displayed selectivity towards cells with MDR characteristics and produced a similar effect on the microtubule network in investigated cell lines. To understand how CKT0353 might interact with the microtubules, docking experiments were performed. The analysis showed that CKT0353 binds well at the nocodazole binding domain of β-tubulin, with good Gibbs free energy (ΔG) values (-6.5 kcal/mol) (Fig. 5) when compared to nocodazole (−5.9 kcal/mol) (Online Resource 1 Fig. 3). The overlap between CKT0353 and Noc is substantial and both compounds likely share this binding site on β-tubulin (Online Resource 1 Fig. 3).

MDR cancer cells do not show resistance to CKT0353

The investigated cervix and breast cancer cell lines, HeLa and T-47D, displayed high sensitivity towards CKT0353 with GI_{50} values in the nanomolar range [18].

However, different cancer cells may express resistance to drugs that target microtubules. A discovery of novel MTAs with the ability to circumvent various multidrug resistance mechanisms is vital for cancer treatment. For this reason, the biological activity of CKT0353 was also tested in a pair of sensitive and multidrug resistant colorectal carcinoma cell lines, DLD1 and DLD1-TxR. Resistant DLD1-TxR cells were selected from DLD1 cells after long-term selective pressure of another MTA, paclitaxel. MDR mechanisms of DLD1-TxR cells acquired after PTX exposure include significantly increased P-gp expression and activity as well as decreased expression of the βIII-tubulin isoform [15].

The effect of CKT0353 on cell growth in colorectal carcinoma DLD1 and their MDR counterpart DLD1-TxR was evaluated by SRB assay. The results obtained after 48 h of treatment were compared to nocodazole as well as other well-known microtubule targeting agents (Table 1). CKT0353 had a prominent antiproliferative effect against colorectal carcinoma cells with GI_{50} values in the micromolar range. More importantly, CKT0353 displayed higher efficacy towards MDR colorectal carcinoma cells. Similar result was also observed with Noc treatment. In comparison, we previously reported that MDR DLD1-TxR cells demonstrate resistance to MTAs such as PTX, vinblastine and colchicine [15]. The relative resistance factor (Rf), expressed as the ratio of GI_{50} values between MDR and sensitive cells, was used to determine the level of resistance (Table 1). DLD1-TxR cells demonstrated moderate resistance to colchicine (Rf = 9.1), and considerable resistance to vinblastine (Rf = 20) and paclitaxel (Rf = 45). The GI_{50} values obtained after CKT0353 treatment in DLD1 and DLD1-TxR cells were 11.4 μM and 5.3 μM, respectively (Rf = 0.46). The GI_{50} values obtained after Noc treatment in DLD1 and DLD1-TxR cells were 0.41 μM and 0.11 μM, respectively (Rf = 0.27). Higher Noc sensitivity in MDR DLD1-TxR cells is likely due to Noc having the lowest affinity for βIII-tubulin [38], an isoform more abundantly expressed in the parental colorectal carcinoma cell line.

Interestingly, we previously showed that another colorectal carcinoma cell line, WiDr, showed considerably higher sensitivity to CKT0353 compared to DLD1 [18]. It has been reported that sensitivity to microtubule depolymerizing drugs, nocodazole and griseofulvin, is strongly connected to aneuploidy in colorectal carcinoma cell lines [39]. WiDr cells possess an aneuploid karyotype [40], and aneuploid cell lines with unstable centrosomes display higher sensitivity to these agents compared to diploid cell lines (DLD1) [39,41]. It is possible that the difference in sensitivity to CKT0353 between WiDr and DLD1 colorectal carcinoma cells could be, at least partially, associated to this phenomenon. In that respect, an aneuploid karyotype in HeLa and T-47D cell lines could also be connected to their CKT0353 sensitivity to a certain extent.

CKT0353 does not influence P-gp activity in MDR cancer cells

P-gp overexpression in MDR cancer cells reduces the intracellular concentration of its substrates, thus decreasing drug cytotoxicity. While many MTAs like taxanes or colchicine are P-gp substrates, the efficacy of nocodazole is not dependent on its function [42]. P-gp inhibitors could potentially improve drug bioavailability by blocking drug extrusion [43]. Since P-gp overexpressing DLD1-TxR cells showed higher sensitivity to CKT0353 compared to sensitive parental cells, the ability of the compound to inhibit the P-gp transporter was evaluated by Rho123 accumulation assay (Fig. 6a). The effect of CKT0353 on the P-gp function was compared to a well-known P-gp inhibitor verapamil (VER). While the addition of 5 μM VER entirely inhibited the Rho123 efflux from DLD1-TxR cells, the efficacy of 5 μM CKT0353 as a P-gp function modulator was not considerable. This finding demonstrates that CKT0353 does not interact with this efflux pump.

CKT0353 induces cell cycle arrest in MDR cancer cells

Considering that a substantial growth arrest was observed in DLD1-TxR cells after CKT0353 application, we next analyzed how CKT0353 affected cell cycle kinetics in cancer cells with MDR phenotype compared to their sensitive counterpart. The cell cycle

disturbance in DLD1 and DLD1-TxR cells was analyzed by flow cytometry after 24 h and 48 h CKT0353 treatment. The addition of the compound significantly altered the cell cycle kinetics in both colorectal carcinoma cell lines regardless of the MDR phenotype, leading to a considerable cell cycle arrest in G_2/M phase after 24 h treatment (Fig. 6b). Treatment with approximate GI_{50} concentrations of CKT0353 resulted in 83.6% (DLD1) and 86.7% (DLD1-TxR) of cells in G_2/M phase, further confirming high sensitivity of MDR cells to the compound. After 48 h, a portion of DLD1 and DLD1-TxR cells managed to overcome the G_2/M arrest, increasing the percentage of cells in G_0/G_1 and sub-G_1 phase, indicating cell death (Online Resource 1 Fig. 4). Treatment with $3xGI_{50}$ concentrations of CKT0353 showed that the observed effect on the cell cycle was dose-dependent in both cell lines, particularly at 48 h. For comparison, a disturbance in cell cycle kinetics in DLD1 and DLD1-TxR cells after 24 h and 48 h Noc treatment was also evaluated by flow cytometry (Online Resource 1 Fig. 5). Treatment with GI_{50} concentration of Noc produced similar results promoting a significant G_2/M phase arrest after 24 h. However, the Noc effect on cell death was more substantial in both cell lines and the sub-G_1 population was more notable, especially after 48 h.

CKT0353 alters microtubule network in MDR cancer cells

To further investigate the mechanisms behind the G_2/M phase arrest in DLD1 and DLD1-TxR cells after CKT0353 treatment, we evaluated the effect of CKT0353 on microtubule network by fluorescence microscopy (Fig. 7). Sensitive and MDR cells were exposed to CKT0353 (for 24 h or 48 h) or Noc (for 24 h), and immunostained to label β-tubulin. Control cells displayed typical cytoskeleton structures characterized by long and dense microtubules. After 24 h, both cell lines treated with approximate GI_{50} concentrations of CKT0353 showed asymmetrical mitosis with activation of the mitotic spindle checkpoint, a phenotype very similar to the effect of Noc (Fig. 7). Furthermore, the effect of CKT0353 continued after 48 h causing depolymerization of tubulin and the appearance of abnormal microtubules. It was reported that silencing of βIII-tubulin isoform sensitizes non-small cell lung carcinoma [44] and breast carcinoma cells [45] to

PTX and vinca alkaloids, while βIII-tubulin overexpression is associated with lower sensitivity to PTX, docetaxel, epothilone B, and vinblastine in HeLa cells [46]. We previously found that DLD1-TxR cells exhibit a decreased expression of βIII-tubulin and show increased sensitivity to another tubulin interacting agent DTA0100, compared to parental DLD1 cells [15]. Consequently, the altered expression of βIII-tubulin in multidrug resistant DLD1-TxR cells may affect microtubule dynamic and be one of the mechanisms responsible for the increased sensitivity to CKT0353.

Conclusion

Novel MTAs not affected by the common resistance mechanisms could provide new prospects for effective cancer treatment. Herein, we presented the mechanism of CKT0353 action against different cancer cell lines. According to our results, CKT0353 is a microtubule destabilizing agent that binds to nocodazole binding site on β-tubulin. The effectiveness of CKT0353 was not diminished in cancer cells with P-gp overexpression, and MDR cells displayed higher sensitivity to CKT0353 and nocodazole compared to their sensitive counterparts. Thus, CKT0353, as a novel MTA that evades MDR phenotype, could be an excellent candidate for developing new strategies to improve cancer treatment.

Acknowledgements

This work was performed within the framework of COST Action CA17104 STRATAGEM – ”New diagnostic and therapeutic tools against multidrug resistant tumors”.

Compliance with ethical standards

Conflict of interest

Jelena Dinić declares that she has no conflict of interest. Carla Ríos-Luci declares that she has no conflict of interest. Ieva Karpaviciene declares that she has no conflict of

interest. Inga Cikotiene declares that she has no conflict of interest. Miguel X. Fernandes declares that he has no conflict of interest. Milica Pešić declares that she has no conflict of interest. José M. Padrón declares that he has no conflict of interest.

Funding

The work was supported by the Ministry of Education, Science and Technological Development of the Republic of Serbia (Grant No. III41031), the EU Research Potential (FP7-REGPOT- 2012-CT2012-31637-IMBRAIN), and the European Social Fund under the Global Grant measure (Grant No. VP1-3.1-ŠMM-07-K-01-002).

Ethical approval

This article does not contain any studies with human participants or animals performed by any of the authors.

Informed consent

For this type of study, formal consent is not required.

References

1. Zhou J, Giannakakou P (2005) Targeting microtubules for cancer chemotherapy. Current medicinal chemistry Anti-cancer agents 5 (1):65-71

2. Jordan MA, Wilson L (2004) Microtubules as a target for anticancer drugs. Nature reviews Cancer 4 (4):253-265. doi:10.1038/nrc1317

3. Downing KH (2000) Structural basis for the interaction of tubulin with proteins and drugs that affect microtubule dynamics. Annual review of cell and developmental biology 16:89-111. doi:10.1146/annurev.cellbio.16.1.89

4. Gottesman MM, Fojo T, Bates SE (2002) Multidrug resistance in cancer: role of ATP-dependent transporters. Nature reviews Cancer 2 (1):48-58. doi:10.1038/nrc706

5. Riordan JR, Ling V (1985) Genetic and biochemical characterization of multidrug resistance. Pharmacology & therapeutics 28 (1):51-75

6. Sharom FJ (2008) ABC multidrug transporters: structure, function and role in chemoresistance. Pharmacogenomics 9 (1):105-127. doi:10.2217/14622416.9.1.105

7. Ambudkar SV, Dey S, Hrycyna CA, Ramachandra M, Pastan I, Gottesman MM (1999) Biochemical, cellular, and pharmacological aspects of the multidrug transporter. Annual review of pharmacology and toxicology 39:361-398. doi:10.1146/annurev.pharmtox.39.1.361

8. Gonzalez-Garay ML, Chang L, Blade K, Menick DR, Cabral F (1999) A beta-tubulin leucine cluster involved in microtubule assembly and paclitaxel resistance. The Journal of biological chemistry 274 (34):23875-23882

9. Kavallaris M, Tait AS, Walsh BJ, He L, Horwitz SB, Norris MD, Haber M (2001) Multiple microtubule alterations are associated with Vinca alkaloid resistance in human leukemia cells. Cancer research 61 (15):5803-5809

10. Giannakakou P, Gussio R, Nogales E, Downing KH, Zaharevitz D, Bollbuck B, Poy G, Sackett D, Nicolaou KC, Fojo T (2000) A common pharmacophore for epothilone and taxanes: molecular basis for drug resistance conferred by tubulin mutations in human cancer cells. Proceedings of the National Academy of Sciences of the United States of America 97 (6):2904-2909. doi:10.1073/pnas.040546297

11. Ganapathi RN, Ganapathi MK (2013) Mechanisms regulating resistance to inhibitors of topoisomerase II. Frontiers in pharmacology 4:89. doi:10.3389/fphar.2013.00089

12. McGrogan BT, Gilmartin B, Carney DN, McCann A (2008) Taxanes, microtubules and chemoresistant breast cancer. Biochimica et biophysica acta 1785 (2):96-132. doi:10.1016/j.bbcan.2007.10.004

13. Goncalves A, Braguer D, Kamath K, Martello L, Briand C, Horwitz S, Wilson L, Jordan MA (2001) Resistance to Taxol in lung cancer cells associated with increased microtubule dynamics. Proceedings of the National Academy of Sciences of the United States of America 98 (20):11737-11742. doi:10.1073/pnas.191388598

14. Kavallaris M, Kuo DY, Burkhart CA, Regl DL, Norris MD, Haber M, Horwitz SB (1997) Taxol-resistant epithelial ovarian tumors are associated with altered expression of specific beta-tubulin isotypes. The Journal of clinical investigation 100 (5):1282-1293. doi:10.1172/JCI119642

15. Podolski-Renic A, Bankovic J, Dinic J, Rios-Luci C, Fernandes MX, Ortega N, Kovacevic-Grujicic N, Martin VS, Padron JM, Pesic M (2017) DTA0100, dual topoisomerase II and microtubule inhibitor, evades paclitaxel resistance in P-glycoprotein overexpressing cancer cells. European journal of pharmaceutical sciences : official journal of the European Federation for Pharmaceutical Sciences 105:159-168. doi:10.1016/j.ejps.2017.05.011

16. Zhang CC, Yang JM, Bash-Babula J, White E, Murphy M, Levine AJ, Hait WN (1999) DNA damage increases sensitivity to vinca alkaloids and decreases sensitivity to taxanes through p53-dependent repression of microtubule-associated protein 4. Cancer research 59 (15):3663-3670

17. Zhang CC, Yang JM, White E, Murphy M, Levine A, Hait WN (1998) The role of MAP4 expression in the sensitivity to paclitaxel and resistance to vinca alkaloids in p53 mutant cells. Oncogene 16 (12):1617-1624. doi:10.1038/sj.onc.1201658

18. Karpaviciene I, Cikotiene I, Padron JM (2013) Synthesis and antiproliferative activity of alpha-branched alpha,beta-unsaturated ketones. European journal of medicinal chemistry 70:568-578. doi:10.1016/j.ejmech.2013.10.041

19. Podolski-Renic A, Andelkovic T, Bankovic J, Tanic N, Ruzdijic S, Pesic M (2011) The role of paclitaxel in the development and treatment of multidrug resistant cancer cell lines. Biomedicine & pharmacotherapy = Biomedecine & pharmacotherapie 65 (5):345-353. doi:10.1016/j.biopha.2011.04.015

20. Kepp O, Galluzzi L, Lipinski M, Yuan J, Kroemer G (2011) Cell death assays for drug discovery. Nature reviews Drug discovery 10 (3):221-237. doi:10.1038/nrd3373

21. Bradford MM (1976) A rapid and sensitive method for the quantitation of microgram quantities of protein utilizing the principle of protein-dye binding. Analytical biochemistry 72:248-254

22. Gascoigne KE, Taylor SS (2008) Cancer cells display profound intra- and interline variation following prolonged exposure to antimitotic drugs. Cancer cell 14 (2):111-122. doi:10.1016/j.ccr.2008.07.002

23. Rieder CL, Maiato H (2004) Stuck in division or passing through: what happens when cells cannot satisfy the spindle assembly checkpoint. Developmental cell 7 (5):637-651. doi:10.1016/j.devcel.2004.09.002

24. Nakano H, Wang W, Hashizume C, Funasaka T, Sato H, Wong RW (2011) Unexpected role of nucleoporins in coordination of cell cycle progression. Cell cycle 10 (3):425-433. doi:10.4161/cc.10.3.14721

25. Fernandez-Martinez J, Rout MP (2009) Nuclear pore complex biogenesis. Current opinion in cell biology 21 (4):603-612. doi:10.1016/j.ceb.2009.05.001

26. Michel L, Diaz-Rodriguez E, Narayan G, Hernando E, Murty VV, Benezra R (2004) Complete loss of the tumor suppressor MAD2 causes premature cyclin B degradation and mitotic failure in human somatic cells. Proceedings of the National Academy of Sciences of the United States of America 101 (13):4459-4464. doi:10.1073/pnas.0306069101

27. Decordier I, Cundari E, Kirsch-Volders M (2008) Mitotic checkpoints and the maintenance of the chromosome karyotype. Mutation research 651 (1-2):3-13. doi:10.1016/j.mrgentox.2007.10.020

28. Lampson MA, Kapoor TM (2005) The human mitotic checkpoint protein BubR1 regulates chromosome-spindle attachments. Nature cell biology 7 (1):93-98. doi:10.1038/ncb1208

29. Sudakin V, Chan GK, Yen TJ (2001) Checkpoint inhibition of the APC/C in HeLa cells is mediated by a complex of BUBR1, BUB3, CDC20, and MAD2. The Journal of cell biology 154 (5):925-936. doi:10.1083/jcb.200102093

30. Dalton WB, Yang VW (2009) Role of prolonged mitotic checkpoint activation in the formation and treatment of cancer. Future oncology 5 (9):1363-1370. doi:10.2217/fon.09.118

31. Israels ED, Israels LG (2000) The cell cycle. The oncologist 5 (6):510-513

32. Harvey SL, Charlet A, Haas W, Gygi SP, Kellogg DR (2005) Cdk1-dependent regulation of the mitotic inhibitor Wee1. Cell 122 (3):407-420. doi:10.1016/j.cell.2005.05.029

33. Blagosklonny MV (2007) Mitotic arrest and cell fate: why and how mitotic inhibition of transcription drives mutually exclusive events. Cell cycle 6 (1):70-74. doi:10.4161/cc.6.1.3682

34. Janicke RU, Sprengart ML, Wati MR, Porter AG (1998) Caspase-3 is required for DNA fragmentation and morphological changes associated with apoptosis. The Journal of biological chemistry 273 (16):9357-9360

35. Walensky LD (2006) BCL-2 in the crosshairs: tipping the balance of life and death. Cell death and differentiation 13 (8):1339-1350. doi:10.1038/sj.cdd.4401992

36. Stanton RA, Gernert KM, Nettles JH, Aneja R (2011) Drugs that target dynamic microtubules: a new molecular perspective. Medicinal research reviews 31 (3):443-481. doi:10.1002/med.20242

37. Jordan MA, Thrower D, Wilson L (1992) Effects of vinblastine, podophyllotoxin and nocodazole on mitotic spindles. Implications for the role of microtubule dynamics in mitosis. Journal of cell science 102 (Pt 3):401-416

38. Xu K, Schwarz PM, Ludueña RF (2002) Interaction of nocodazole with tubulin isotypes. Drug development research 55 (2):91-96

39. Ghadimi BM, Sackett DL, Difilippantonio MJ, Schrock E, Neumann T, Jauho A, Auer G, Ried T (2000) Centrosome amplification and instability occurs exclusively in aneuploid, but not in diploid colorectal cancer cell lines, and correlates with numerical chromosomal aberrations. Genes, chromosomes & cancer 27 (2):183-190

40. Tsushimi T, Noshima S, Oga A, Esato K, Sasaki K (2001) DNA amplification and chromosomal translocations are accompanied by chromosomal instability: analysis of seven human colon cancer cell lines by comparative genomic hybridization and spectral karyotyping. Cancer genetics and cytogenetics 126 (1):34-38

41. Podolski-Renic A, Jadranin M, Stankovic T, Bankovic J, Stojkovic S, Chiourea M, Aljancic I, Vajs V, Tesevic V, Ruzdijic S, Gagos S, Tanic N, Pesic M (2013) Molecular and cytogenetic changes in multi-drug resistant cancer cells and their influence on new

compounds testing. Cancer chemotherapy and pharmacology 72 (3):683-697. doi:10.1007/s00280-013-2247-1

42. Chen Y, Simon SM (2000) In situ biochemical demonstration that P-glycoprotein is a drug efflux pump with broad specificity. The Journal of cell biology 148 (5):863-870

43. Abdallah HM, Al-Abd AM, El-Dine RS, El-Halawany AM (2015) P-glycoprotein inhibitors of natural origin as potential tumor chemo-sensitizers: A review. Journal of advanced research 6 (1):45-62. doi:10.1016/j.jare.2014.11.008

44. Kavallaris M, Burkhart CA, Horwitz SB (1999) Antisense oligonucleotides to class III beta-tubulin sensitize drug-resistant cells to Taxol. British journal of cancer 80 (7):1020-1025. doi:10.1038/sj.bjc.6690507

45. Stengel C, Newman SP, Leese MP, Potter BV, Reed MJ, Purohit A (2010) Class III beta-tubulin expression and in vitro resistance to microtubule targeting agents. British journal of cancer 102 (2):316-324. doi:10.1038/sj.bjc.6605489

46. Risinger AL, Jackson EM, Polin LA, Helms GL, LeBoeuf DA, Joe PA, Hopper-Borge E, Luduena RF, Kruh GD, Mooberry SL (2008) The taccalonolides: microtubule stabilizers that circumvent clinically relevant taxane resistance mechanisms. Cancer research 68 (21):8881-8888. doi:10.1158/0008-5472.CAN-08-2037

Figure legends

Fig. 1 The effect of CKT0353 treatment on cell cycle in HeLa and T-47D cells (**a**) Chemical structure of (*E*)-2-(4-methoxybenzylidene)-4-methylene-1,5-diphenylpentane-1,5-dione (CKT0353). (**b**) CKT0353 induces G_2/M arrest in HeLa and T-47D cells after 24 h and 48 h treatment. Cell cycle stage was determined by flow cytometric analysis of DNA content in individual cells. Representative flow cytometric profiles for each condition are shown.

Fig. 2 CKT0353 treatment induces mitotic slippage in HeLa and T-47D cells (**a**) Induction of mitotic slippage in HeLa and T-47D cells after prolonged CKT0353 exposure. Cells were treated with 0.9 μM CKT0353 for 24 h and 48 h. Nuclear pore complex re-

formation in cells upon mitotic slippage with the appearance of micronucleated cells in a tetraploid G_0 state. HeLa cells scale bar: 10 μm. T-47D cells scale bar: 7.5 μm. (**b**) Western blot analysis of time-dependent expression of pH3, cyclin B1, Cdc2, pCdc2, CDK1, pCDK1, BubR1, pBuBR1, pRb (ser807/811), and Wee1 in HeLa and T-47D cells after 0.9 μM CKT0353 treatment. GAPDH and calnexin were used as protein loading controls.

Fig. 3 The effect of CKT0353 treatment on cell death in HeLa and T-47D cells (**a**) CKT0353 induces apoptotic cell death in HeLa cells. Representative flow cytometric profiles of AV/PI stained cells for each condition are presented. (**b**) CKT0353 triggers loss of mitochondrial membrane potential in HeLa cells. HeLa and T-47D cells were treated with CKT0353 for the indicated times and $\Delta\Psi_m$ was evaluated using TMRE. Live single cells were gated and fluorescence intensity decrease of TMRE was quantified by flow cytometry. Representative flow cytometric profiles for each condition are shown. Histograms show average percentages of TMRE positive cells from three independent experiments. (**c**) CKT0353 caused cell death in HeLa cells through a caspase-dependent mechanism. HeLa and T-47D cells were treated for the indicated times with CKT0353 and the expression of PARP-1, caspase 3, caspase 7, caspase 9, Mcl-1, and Bcl-2 were analyzed by Western blotting. GAPDH and calnexin were used as protein loading controls.

Fig. 4 CKT0353 disrupts the mitotic spindle in HeLa and T-47D cells The cells were treated with CKT0353 (24 h or 48 h) or Noc (24 h), fixed and stained with anti β-tubulin antibody (green), while the nuclei were counterstained with DAPI (blue). Representative confocal images are shown. HeLa cells scale bar: 10 μm. T-47D cells scale bar: 7.5 μm.

Fig. 5 CKT0353 docked at the nocodazole binding site of β-tubulin

Fig. 6 The effect of CKT0353 treatment on P-glycoprotein function and cell cycle in DLD1 and DLD1-TxR cells (**a**) CKT0353 does not inhibit the P-glycoprotein function. A representative flow cytometric profile of Rho123 accumulation in DLD1 and multidrug

resistant DLD1-TxR cells is shown. Acute P-gp inhibition was monitored in MDR cells treated for 30 min with 5 µM CKT0353 or VER. A minimum of 10,000 events were collected for each experimental sample. (**b**) CKT0353 induces G_2/M arrest in DLD1 and multidrug resistant DLD1-TxR cells after 24 h and 48 h treatment. Cell cycle stage was determined by flow cytometric analysis of DNA content in individual cells. Flow cytometric profiles for each condition are shown.

Fig. 7 CKT0353 disrupts the mitotic spindle in DLD1 and DLD1-TxR cells The cells were treated with CKT0353 (24 h or 48 h) or Noc (24 h), fixed and stained with anti β-tubulin antibody (green), while the nuclei were counterstained with DAPI (blue). Representative confocal images are shown. Scale bar: 25 µm.

Fig. 1

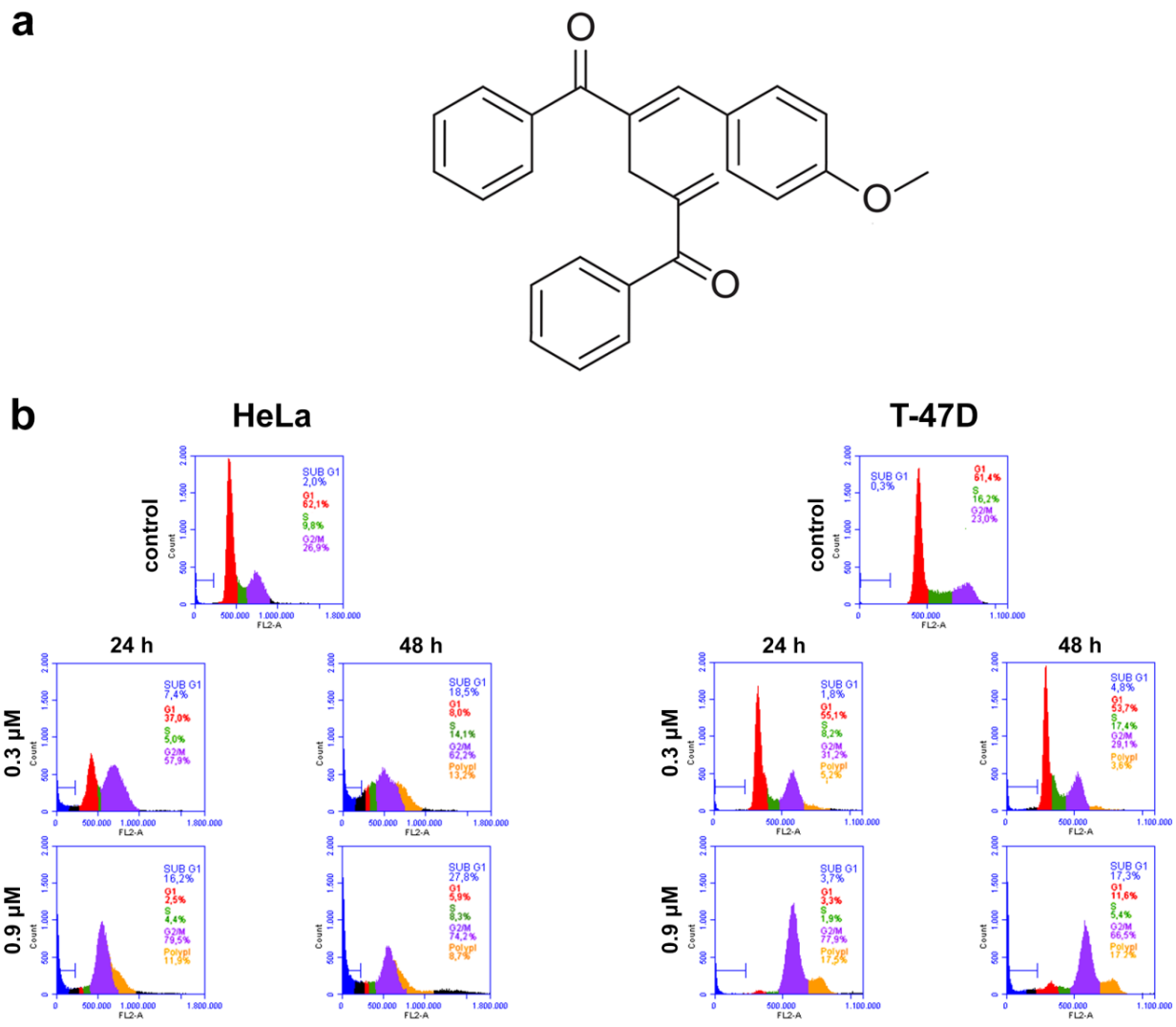
a
O
O
O
b
HeLa
T-47D
control
control
24 h
48 h
24 h
48 h
0.3 µM
0.9 µM
0.3 µM
0.9 µM
SUB G1 2,0%
G1 62,1%
S 9,8%
G2/M 26,9%
SUB G1 0,3%
G1 61,4%
S 16,2%
G2/M 23,0%
SUB G1 7,4%
G1 37,0%
S 5,0%
G2/M 57,9%
SUB G1 18,5%
G1 8,0%
S 14,1%
G2/M 62,2%
Polypl 13,2%
SUB G1 1,8%
G1 55,1%
S 8,2%
G2/M 31,2%
Polypl 5,2%
SUB G1 4,8%
G1 53,7%
S 17,4%
G2/M 28,1%
Polypl 3,8%
SUB G1 16,2%
G1 2,5%
S 4,4%
G2/M 79,5%
Polypl 11,9%
SUB G1 27,8%
G1 5,9%
S 8,3%
G2/M 74,2%
Polypl 8,7%
SUB G1 3,7%
G1 3,3%
S 1,9%
G2/M 77,9%
Polypl 17,5%
SUB G1 17,3%
G1 11,6%
S 5,4%
G2/M 66,5%
Polypl 17,7%
Count
FL2-A

Fig. 2

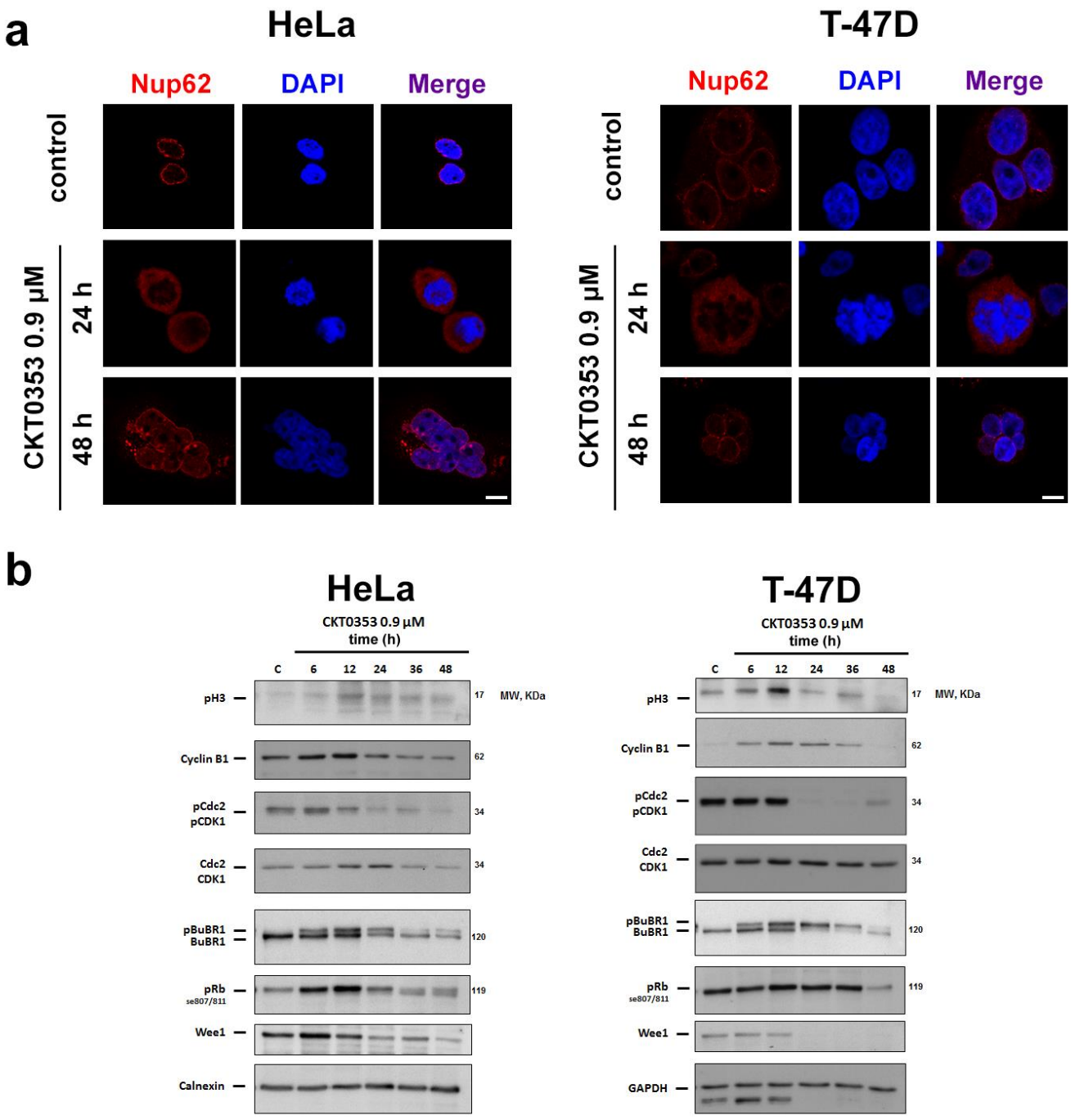
a
HeLa
T-47D
Nup62
DAPI
Merge
control
CKT0353 0.9 µM
24 h
48 h
b
HeLa
T-47D
CKT0353 0.9 µM
time (h)
C
6
12
24
36
48
MW, KDa
pH3
17
Cyclin B1
62
pCdc2
pCDK1
34
Cdc2
CDK1
34
pBuBR1
BuBR1
120
pRb
se807/811
119
Wee1
Calnexin
GAPDH

Fig. 3

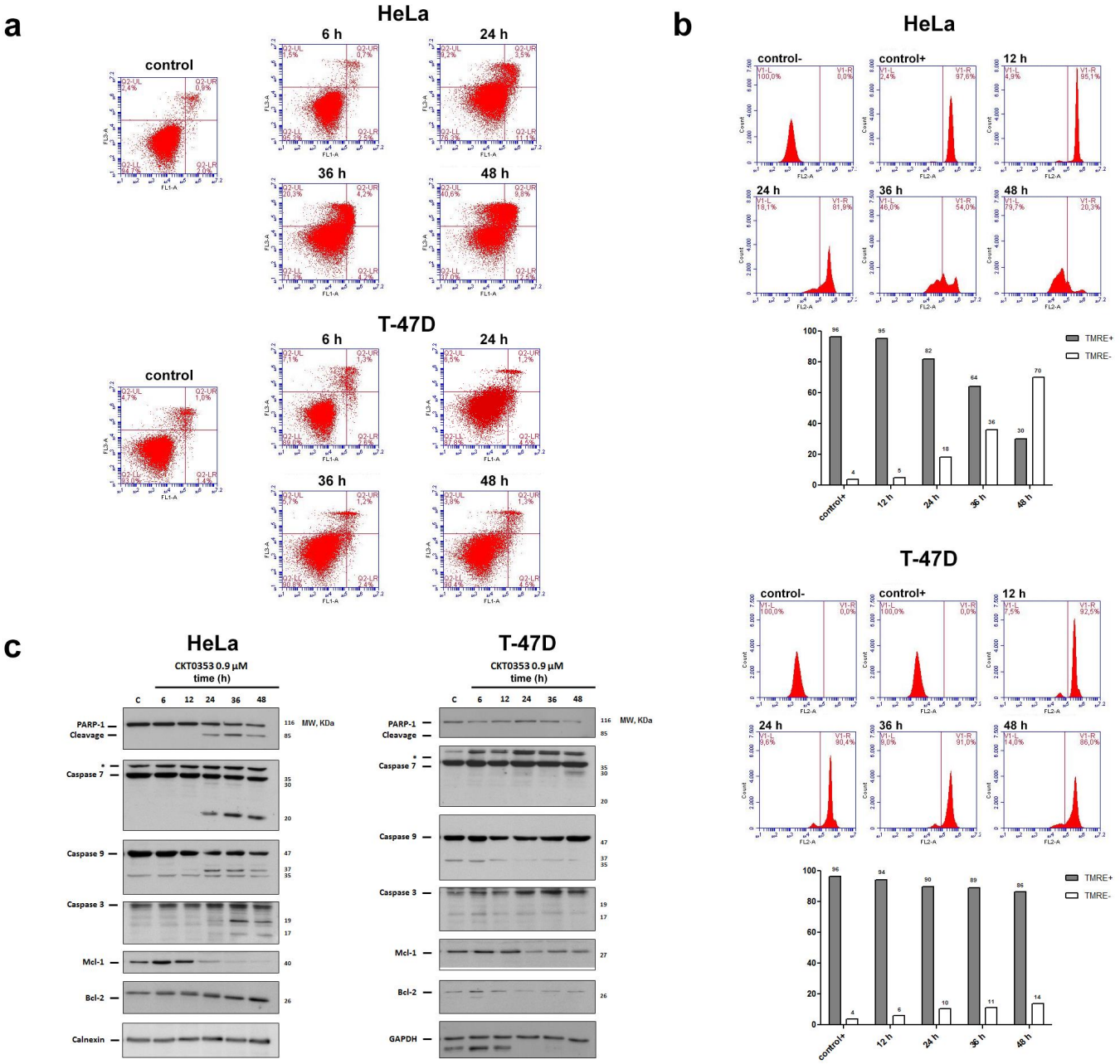
a
HeLa
control
6 h
24 h
36 h
48 h
T-47D
control
6 h
24 h
36 h
48 h
b
HeLa
control-
control+
12 h
24 h
36 h
48 h
TMRE+
TMRE-
control+
12 h
24 h
36 h
48 h
T-47D
control-
control+
12 h
24 h
36 h
48 h
TMRE+
TMRE-
control+
12 h
24 h
36 h
48 h
c
HeLa
CKT0353 0.9 µM
time (h)
C
6
12
24
36
48
PARP-1
Cleavage
Caspase 7
Caspase 9
Caspase 3
Mcl-1
Bcl-2
Calnexin
MW, KDa
T-47D
CKT0353 0.9 µM
time (h)
C
6
12
24
36
48
PARP-1
Cleavage
Caspase 7
Caspase 9
Caspase 3
Mcl-1
Bcl-2
GAPDH
MW, KDa

Fig. 4

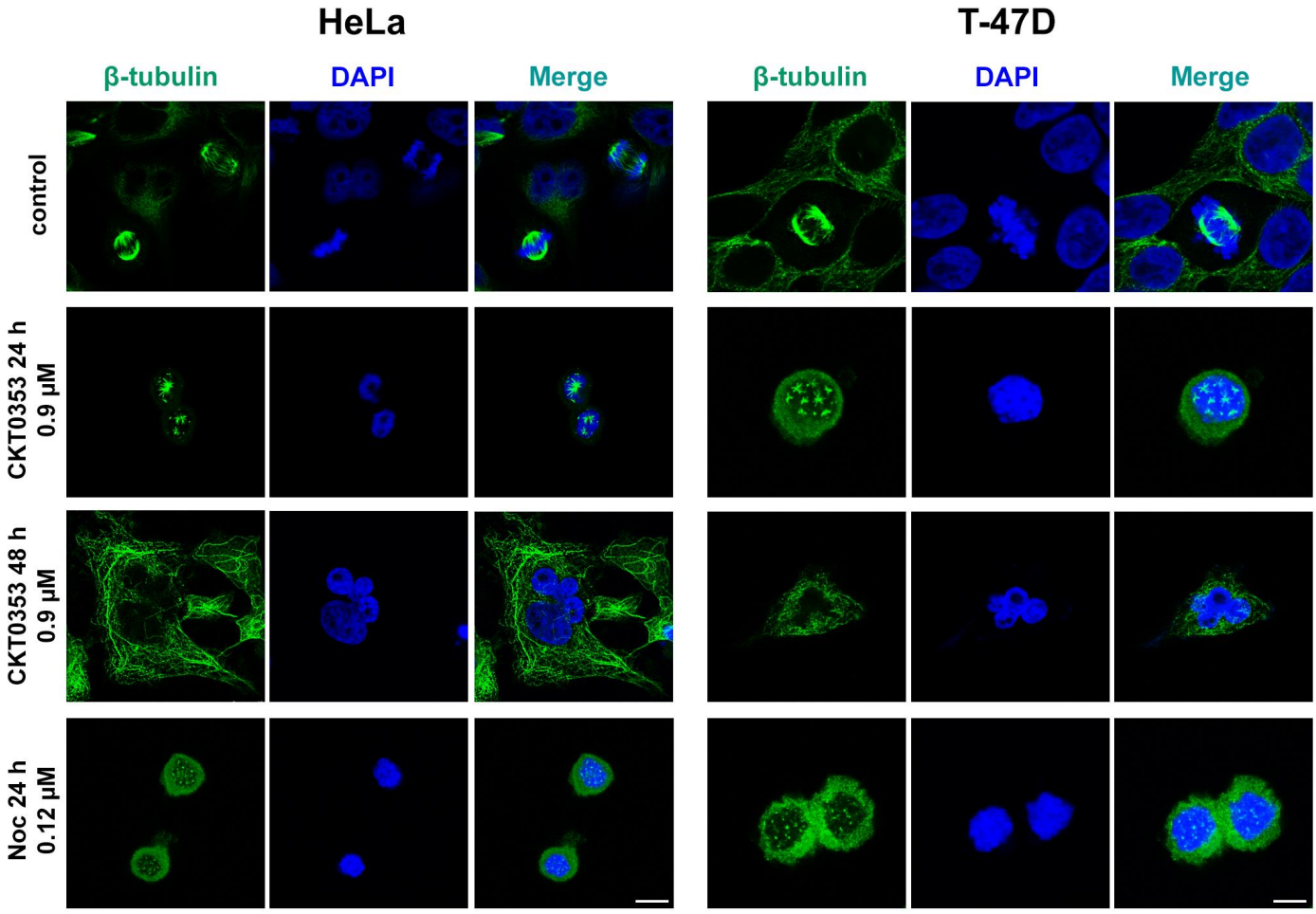
HeLa
T-47D
β-tubulin
DAPI
Merge
β-tubulin
DAPI
Merge
control
CKT0353 24 h 0.9 μM
CKT0353 48 h 0.9 μM
Noc 24 h 0.12 μM

Fig. 5

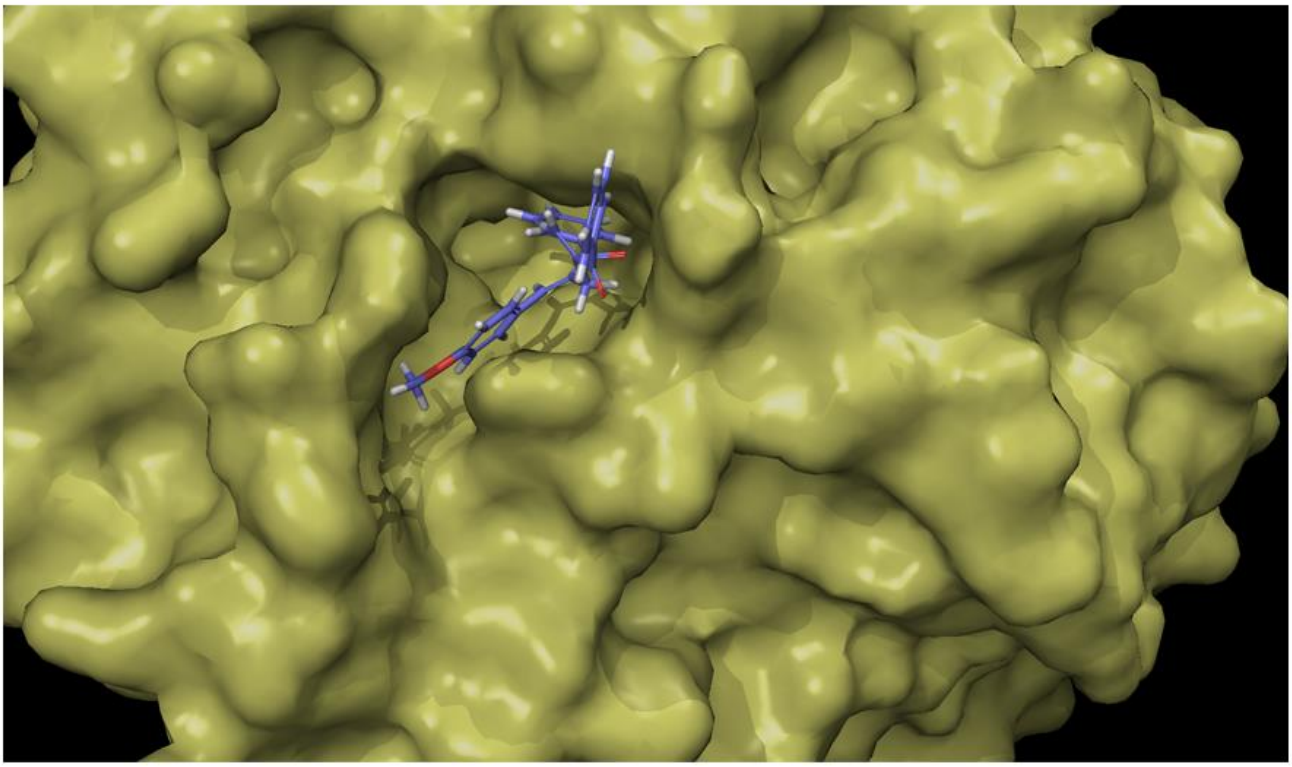

CKT0353 ΔG = −6.5 kcal/mol

Fig. 6

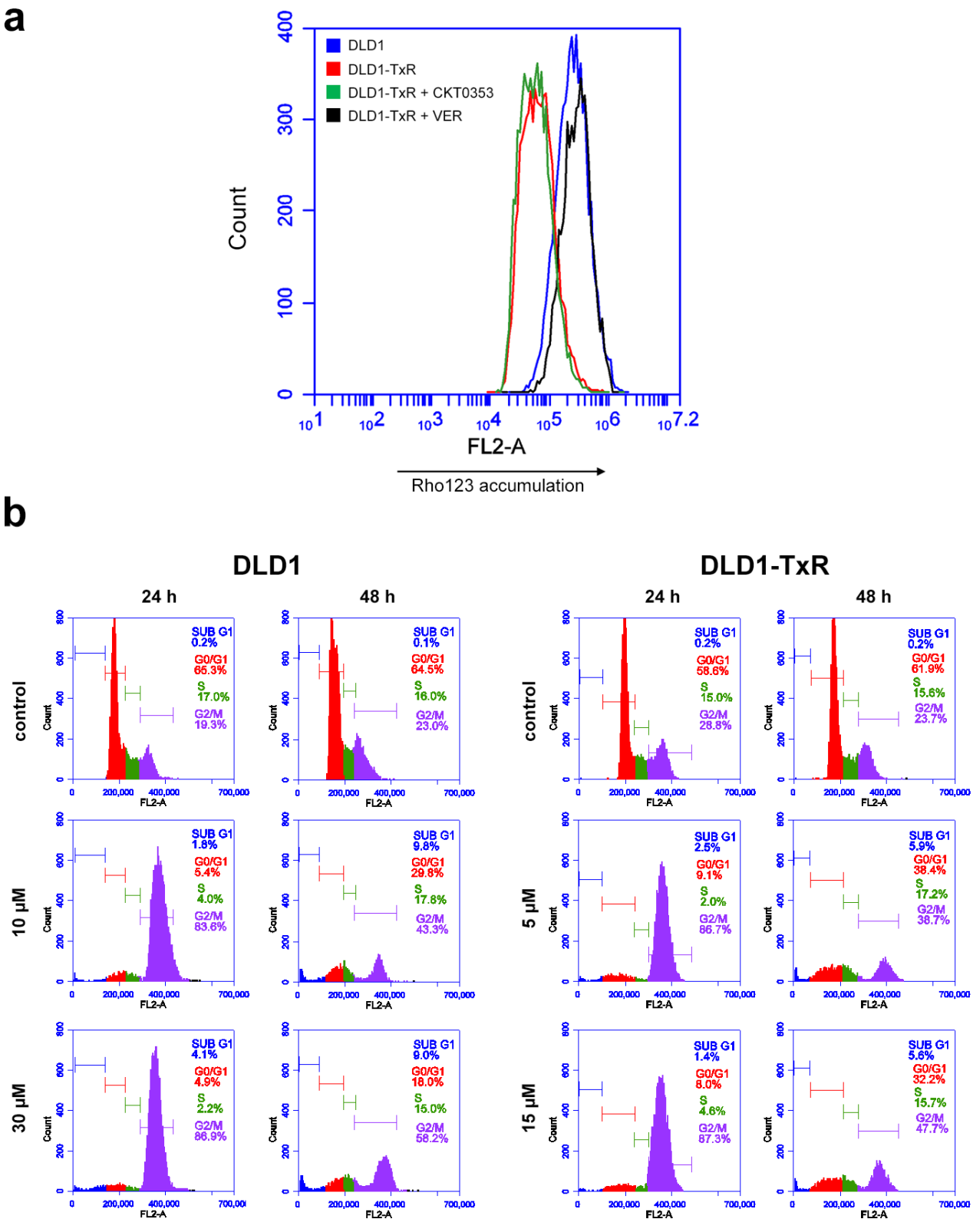
a
DLD1
DLD1-TxR
DLD1-TxR + CKT0353
DLD1-TxR + VER
Count
FL2-A
Rho123 accumulation
b
DLD1
DLD1-TxR
24 h
48 h
control
10 µM
30 µM
5 µM
15 µM
SUB G1
G0/G1
S
G2/M
FL2-A
Count

Fig. 7

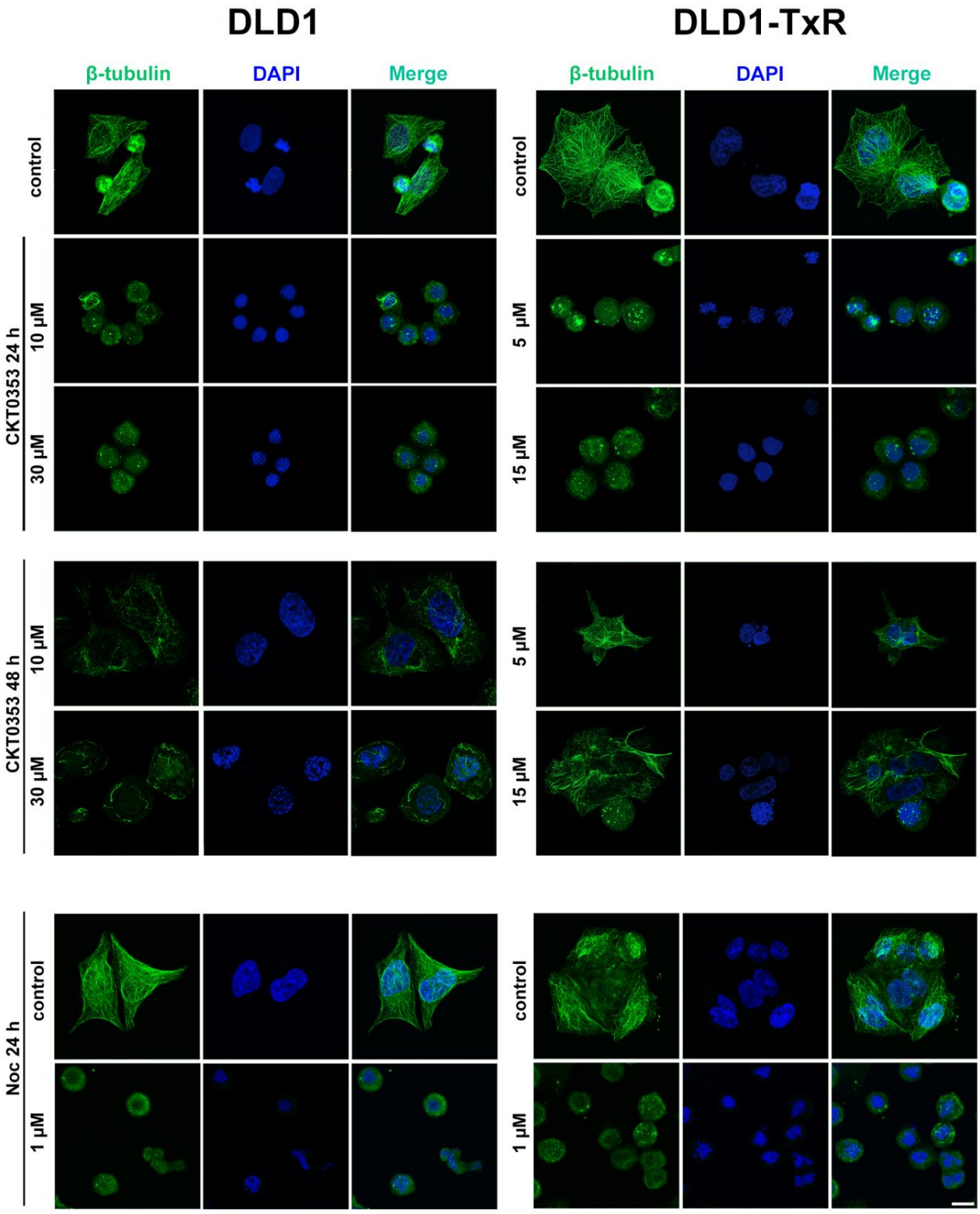
DLD1
DLD1-TxR
β-tubulin
DAPI
Merge
control
CKT0353 24 h
10 μM
30 μM
5 μM
15 μM
CKT0353 48 h
Noc 24 h
1 μM

Table 1 Cross-resistance profile to various microtubule targeting agents obtained by sulforhodamine B assay in DLD1 and DLD1-TxR cells

Drugs	GI_{50} (μM)[a]		Resistance factor[b]
	DLD1	DLD1-TxR	
CKT0353	11.4	5.3	0.46
Nocodazole	0.41	0.11	0.27
Colchicine[15]	0.02	0.17	9.1
Vinblastine[15]	0.01	0.2	20
Paclitaxel[15]	0.04	1.81	45

[a]Values represent the average from three independent experiments

[b]Relative resistance of DLD1-TxR compared to DLD1 cells

Investigational New Drugs - Supplementary Material

CKT0353, a novel microtubule targeting agent, overcomes paclitaxel induced resistance in cancer cells

Jelena Dinić[1*], Carla Ríos-Luci[2], Ieva Karpaviciene[3], Inga Cikotiene[3], Miguel X. Fernandes[2], Milica Pešić[1], José M. Padrón[2*]

[1]Institute for Biological Research "Siniša Stanković", University of Belgrade, Bulevar despota Stefana 142, 11060 Belgrade, Serbia

[2]BioLab, Instituto Universitario de Bio-Organica "Antonio Gonzalez" (IUBO-AG), Centro de Investigaciones Biomédicas de Canarias (CIBICAN), Universidad de La Laguna, Avda. Astrofisico Francisco Sánchez 2, 38206 La Laguna, Tenerife, Spain

[3]Department of Organic Chemistry, Faculty of Chemistry, Vilnius University, Naugarduko 24, Vilnius LT 03225, Lithuania

***Corresponding authors**

Jelena Dinić, PhD

Institute for Biological Research "Siniša Stanković"

University of Belgrade

Bulevar despota Stefana 142, 11 060 Belgrade, Serbia

Tel.: +381 11 20 78 406

Email: jelena.dinic@ibiss.bg.ac.rs

ORCID ID: 0000-0003-3371-2381

José M. Padrón, PhD

BioLab

C/ Astrofísico Francisco Sánchez, 2

38206 La Laguna, Tenerife, Spain

Tel.: + 34 922 316 502 ext. 6126

Email: jmpadron@ull.es

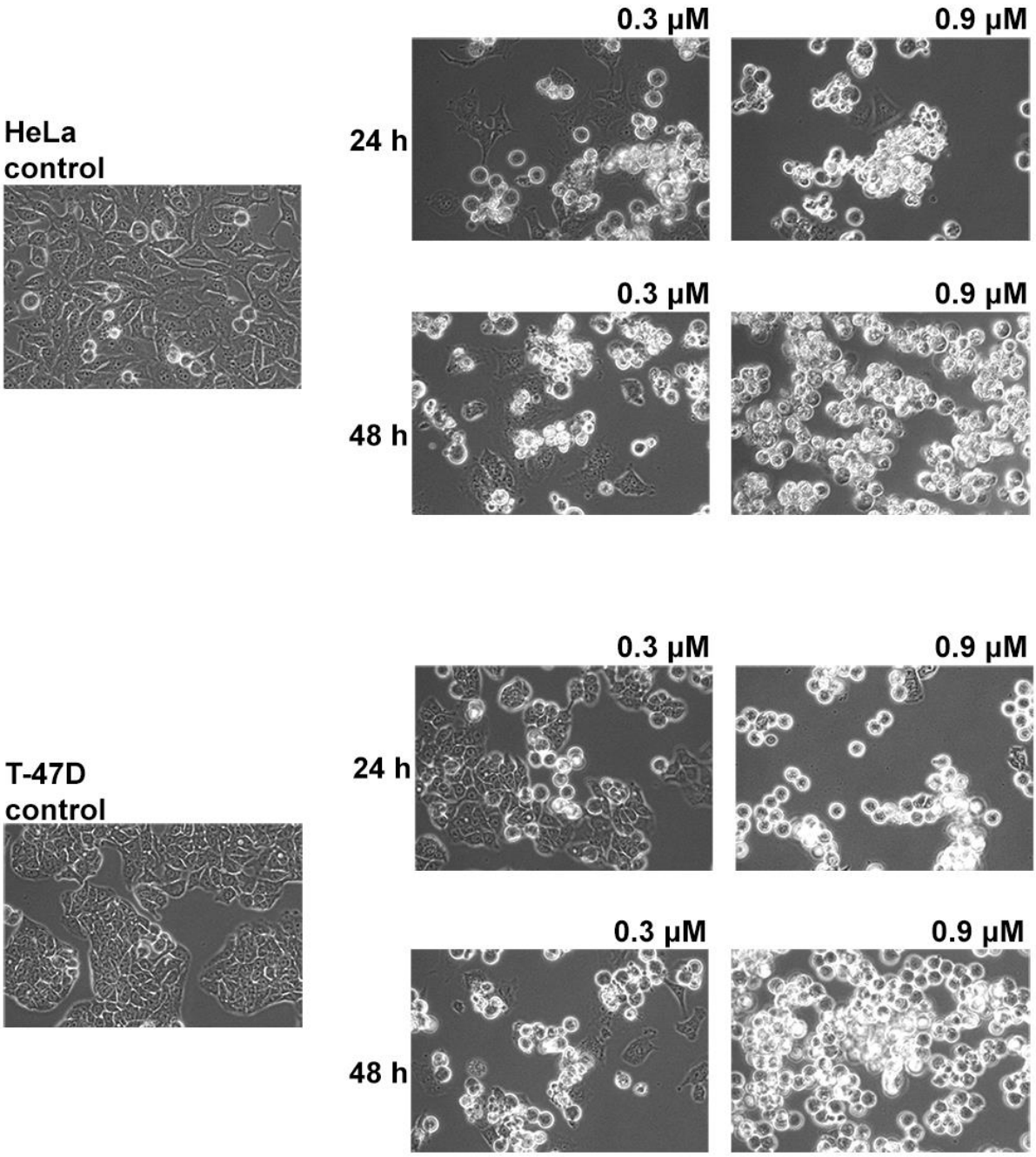

Fig. 1. Morphological changes in HeLa and T-47D cells after CKT0353 treatment HeLa and T-47D cells were treated for 24 h and 48 h with 0.3 µM or 0.9 µM CKT0353.

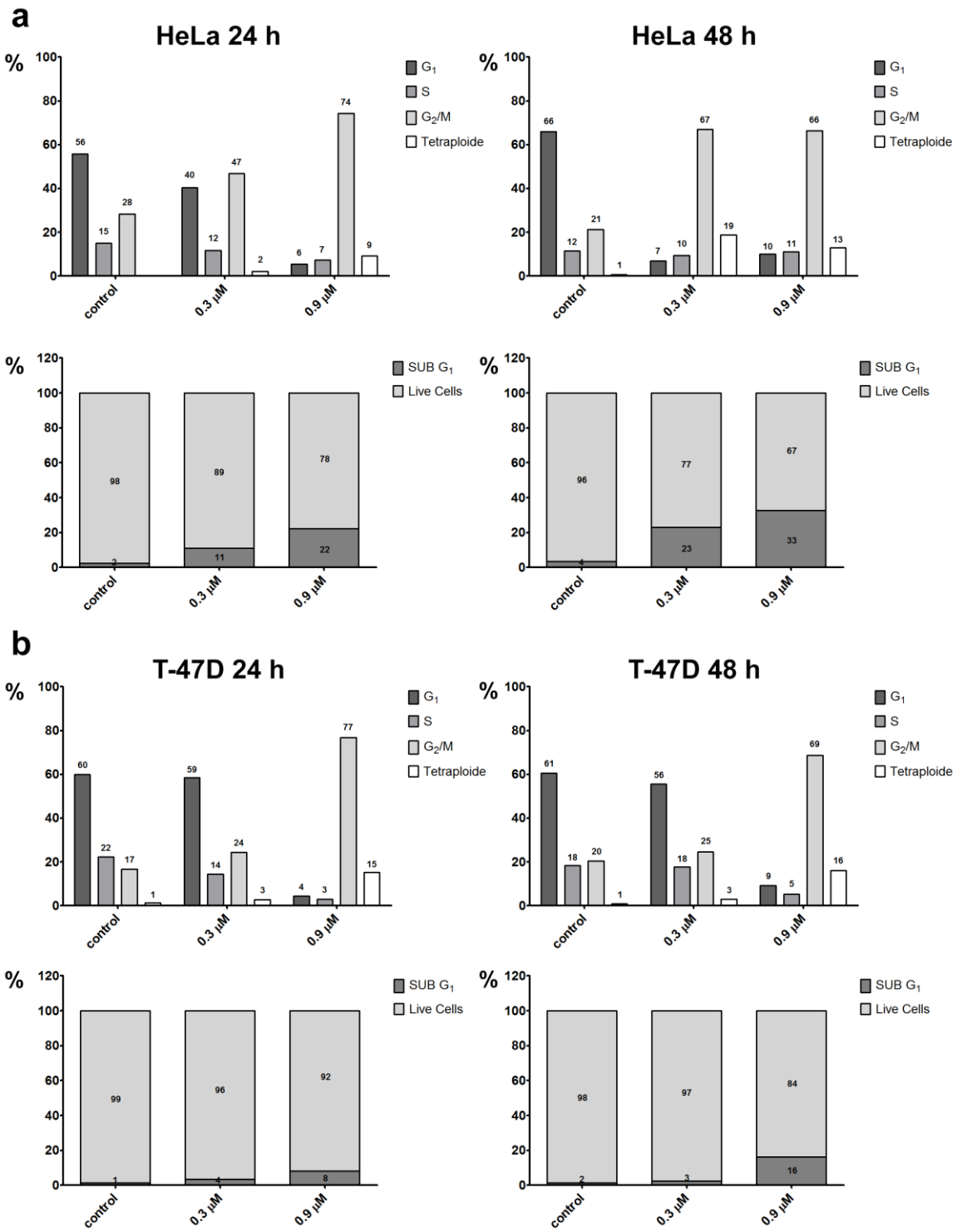

Fig. 2. The effect of CKT0353 treatment on cell cycle in HeLa and T-47D cells (**a**) Percentages of cells in each cell cycle phase of HeLa cells treated with 0.3 µM or 0.9 µM CKT0353. (**b**) Percentages of cells in each cell cycle phase of T-47D cells treated with 0.3 µM or 0.9 µM CKT0353. Average percentages from three independent experiments are presented.

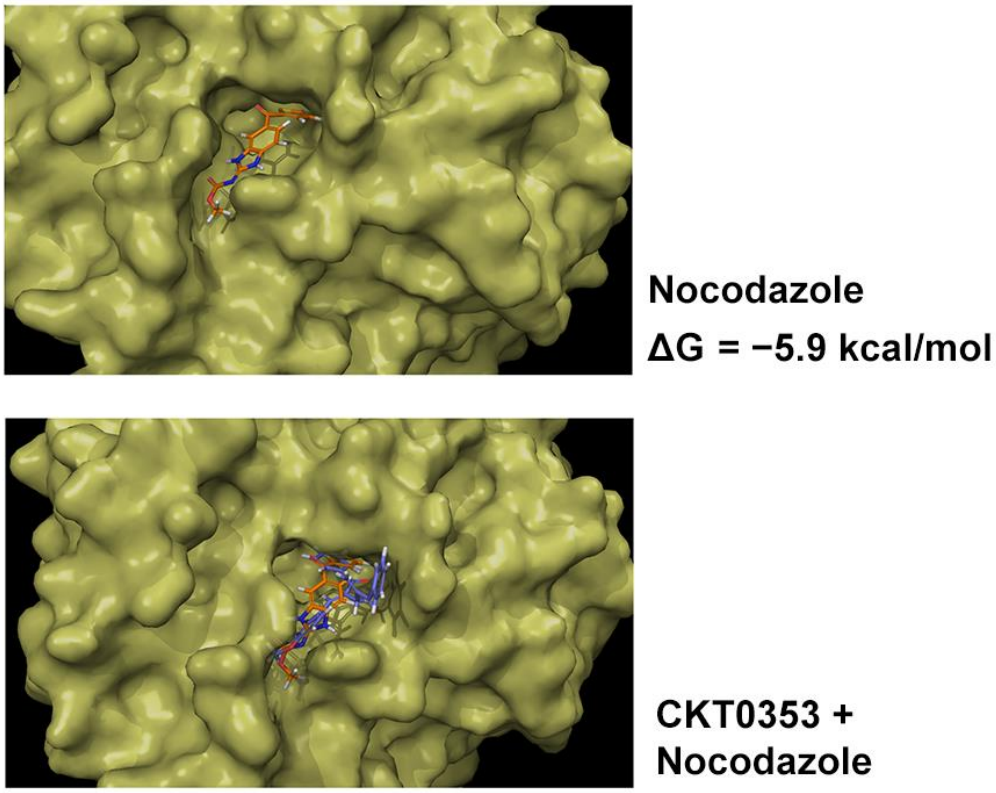

Fig. 3. Comparison of CKT0353 and nocodazole docked at the nocodazole binding site of β-tubulin

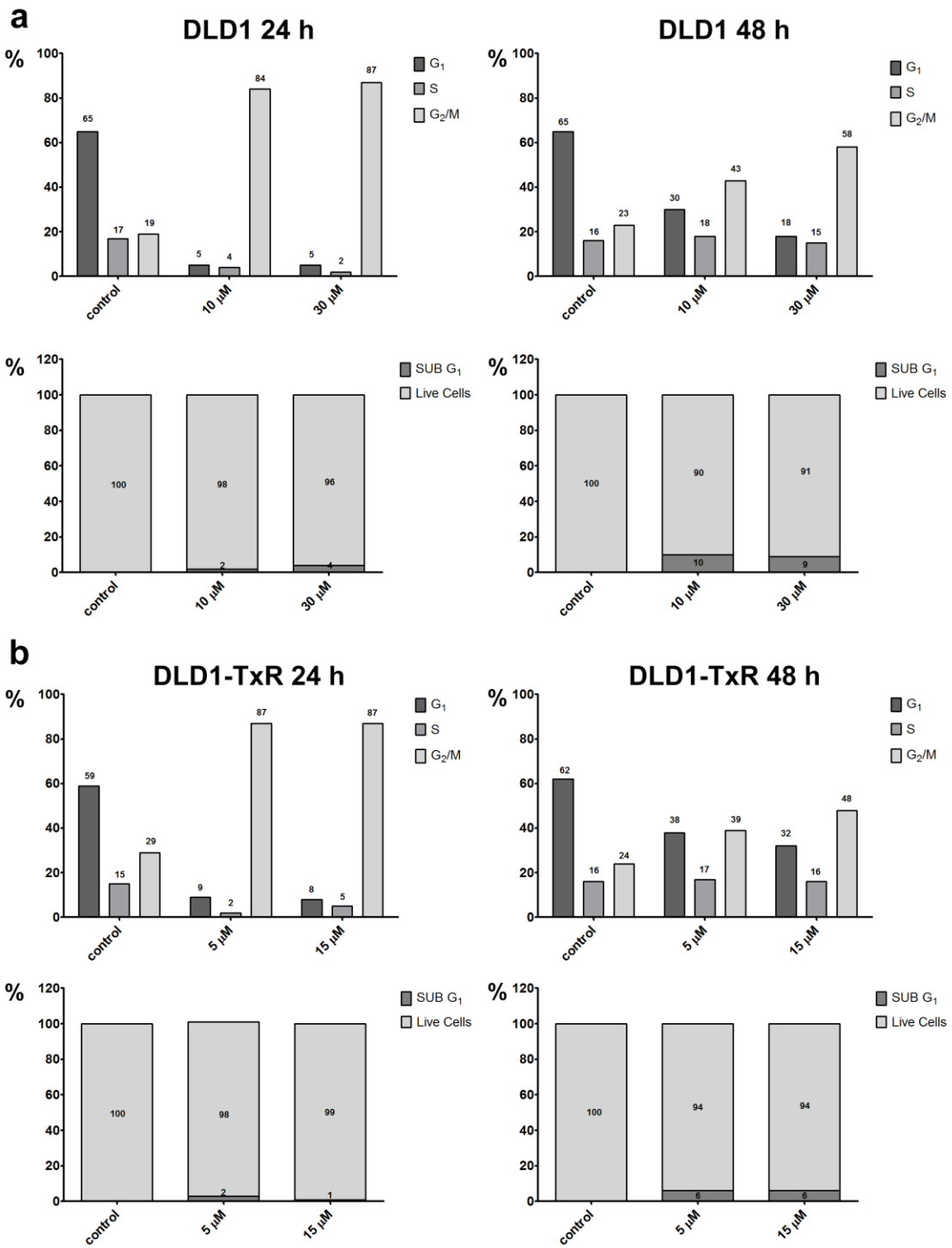

Fig. 4. The effect of CKT0353 treatment on cell cycle in DLD1 and DLD1-TxR cells (**a**) Percentages of cells in each cell cycle phase of DLD1 cells treated with 10 µM or 30 µM CKT0353. (**b**) Percentages of cells in each cell cycle phase of multidrug resistant DLD1-TxR cells treated with 5 µM or 15 µM CKT0353. Average percentages from three independent experiments are presented.

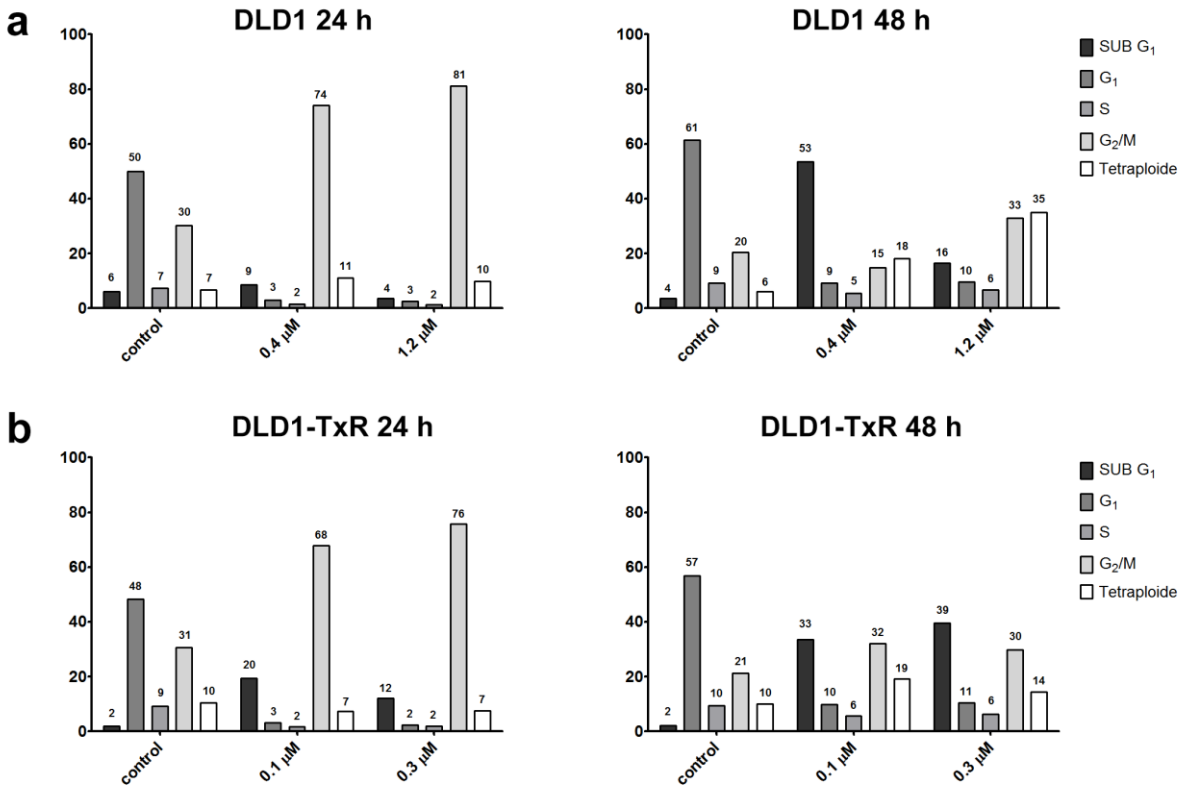

Fig. 5. The effect of nocodazole treatment on cell cycle in DLD1 and DLD1-TxR cells (**a**) Percentages of cells in each cell cycle phase in DLD1 cells treated with 0.4 µM or 1.2 µM Noc. (**b**) Percentages of cells in each cell cycle phase in multidrug resistant DLD1-TxR cells treated with 0.1 µM or 0.3 µM Noc. Representative experiments are presented.

Table 1. CKT0353 induces cell death in HeLa but not in T-47D cells The percentages of live, apoptotic and necrotic cells after treatment with 0.9 µM CKT0353 are presented.

		Live cells (%)	Early apoptosis (%)	Late apoptosis (%)	Necrosis (%)
HeLa	control	94.7	2	0.9	2.4
	6 h	95.3	2.5	0.7	1.5
	24 h	76.3	11.1	3.5	9.2
	36 h	71.3	4.2	4.2	20.3
	48 h	37	12.5	9.8	40.6
T-47D	control	93	1.4	1	4.7
	6 h	89	2.6	1.3	7.1
	24 h	87.8	4.5	1.2	6.5
	36 h	90.8	2.4	1.2	5.7
	48 h	90.4	4.5	1.3	3.8